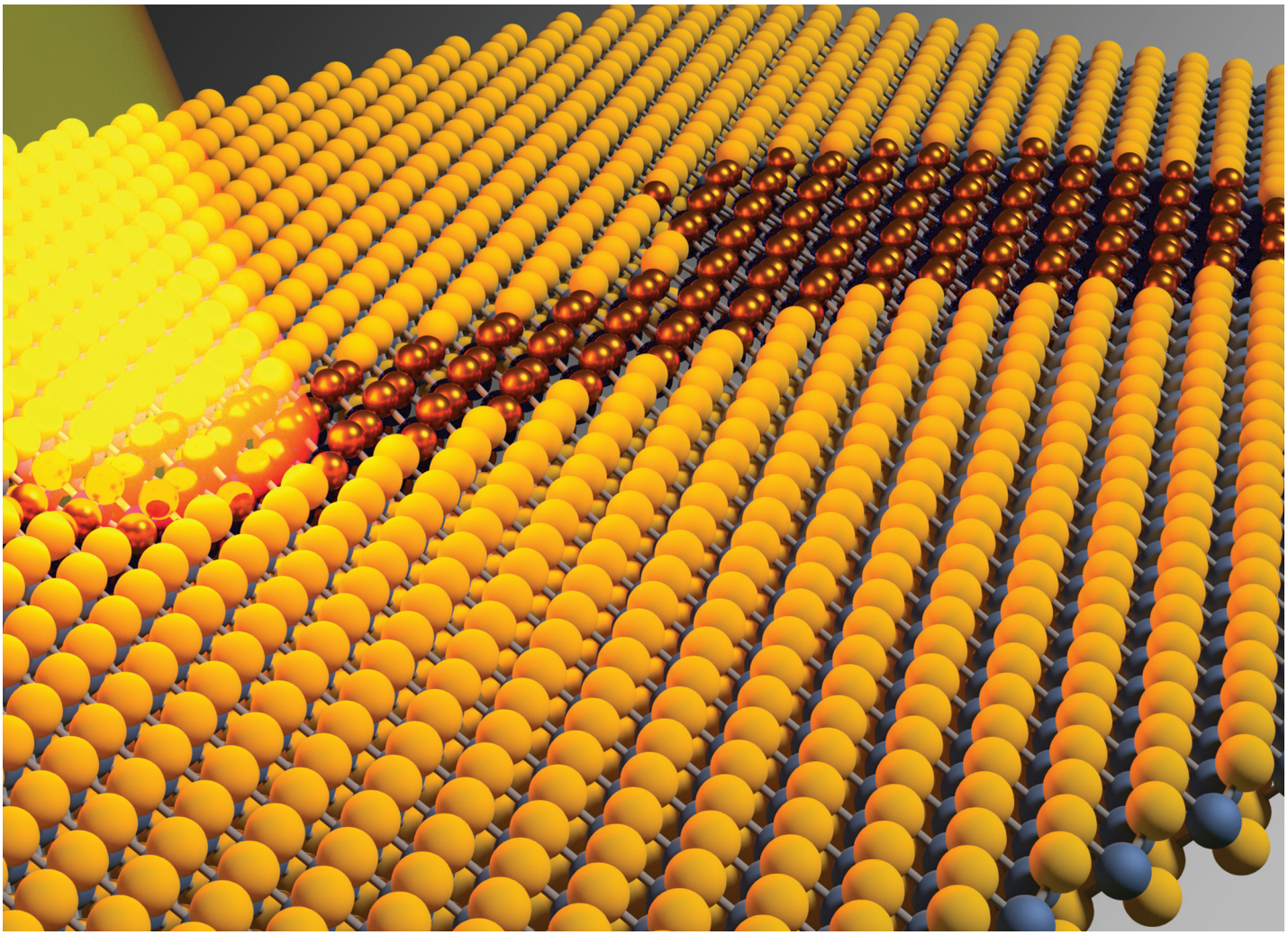

Showcasing research from Collaboratory for Advanced Computing and Simulations (CACS), University of Southern California, Los Angeles, USA.

Semiconductor–metal structural phase transformation in $MoTe_2$ monolayers by electronic excitation

Optical control of transformations between semiconducting and metallic phases of two-dimensional materials can open the door for phase patterning of heterostructures for 2D electronics and catalysis applications. This work shows how optically-induced changes to the electronic structure and Fermi surface of monolayer semiconductors couple to lattice distortions, resulting in a more facile phase transformation pathway. This work highlights photoexcitation as a viable technique for functionalizing these material systems.

As featured in:

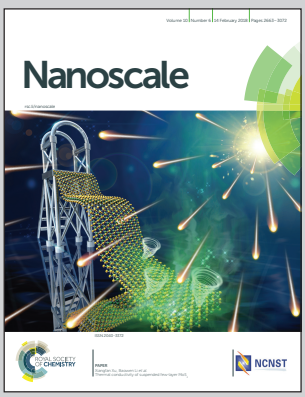

See Aravind Krishnamoorthy *et al.*, *Nanoscale*, 2018, **10**, 2742.

ROYAL SOCIETY OF CHEMISTRY

rsc.li/nanoscale

Registered charity number: 207890

Nanoscale

PAPER

View Article Online
View Journal | View Issue

Cite this: *Nanoscale*, 2018, **10**, 2742

Semiconductor–metal structural phase transformation in $MoTe_2$ monolayers by electronic excitation†

Aravind Krishnamoorthy, *[a] Lindsay Bassman,[a,b] Rajiv K. Kalia,[a,b,c,d] Aiichiro Nakano,[a,b,c,d,e] Fuyuki Shimojo[f] and Priya Vashishta[a,b,c,d]

Received 23rd October 2017,
Accepted 22nd December 2017

DOI: 10.1039/c7nr07890k

rsc.li/nanoscale

Optical modulation of the crystal structure and materials properties is an increasingly important technique for functionalization of two-dimensional and layered semiconductors, where traditional methods like chemical doping are ineffective. Controllable transformation between the semiconducting (H) and semi-metallic (T′) polytypes of transition metal chalcogenide monolayers is of central importance to two-dimensional electronics, and thermally-driven and strain-driven examples of this phase transformation have been previously reported. However, the possibility of a H–T′ phase transformation driven by electronic or optical excitation is less explored and little is known about the potential energy surface and the magnitude of activation barriers or the mechanism of the phase transformation in the excited state. Here, we model the electronic and ionic structure of excited $MoTe_2$ crystals and demonstrate how electronic excitation leads to a Fermi-surface-nesting driven softening of phonon modes at the Brillouin zone boundary and the subsequent stabilization of a low-energy intermediate crystal structure along the semiconductor–metal phase transition pathway. The significantly reduced barriers for this transformation upon electronic excitation suggest that optical excitation may enable rapid and controllable synthesis of lateral semiconductor–metal heterophase homojunctions in monolayer materials for use in next-generation two-dimensional nano-electronics applications.

Introduction

Monolayer transition metal chalcogenide (TMC) crystals of the form MX_2 (M = Mo, W and X = S, Se and Te) can exist in two distinct crystal structures – H and T′, which show very different physical and electronic properties. H polytypes are characterized by a trigonal prismatic arrangement of chalcogen ligands around the central transition metal atom, leading to a direct band-gap semiconductor, whose lack of inversion symmetry leads to valley-selective electronic properties. T′ polytypes have a distorted or twisted octahedral coordination around each transition metal atom and possess inversion symmetry and a semi-metallic electronic structure with complex topological states.[1] Structural transformations between semiconducting H and semi-metallic T′ polytypes of monolayer TMCs are of great interest to the development of two-dimensional electronics,[2–4] optoelectronics,[5,6] sensing[7] and catalysis applications.[8,9] Controllable transformation between the H and T′ phases would enable the formation of defect-free and mechanically-robust[10] semiconductor–metal heterophase homojunctions, which can be used to ensure ohmic contact to two-dimensional semiconductors, where traditional methods developed for bulk 3D semiconductor processing like highly-doped tunnel-contacts are ineffective.[8,11] Significant effort has been made to understand the global (*i.e.* not local) transformation between the H and T′ phases driven by thermal annealing,[12] alloying,[13–19] adsorption,[20] strain engineering[4,10] and electron injection and charge doping[21–24] using experimental and theoretical methods.

In contrast, optically induced electronic excitation is an under-investigated method for controlling the potential energy surface and enabling facile lattice distortions in TMCs. In addition to taking advantage of reduced activation barriers in the excited state for faster phase transformation, optical excitation also offers precise sub-micron control over the for-

[a]*Collaboratory for Advanced Computing and Simulations, University of Southern California, Los Angeles, CA 90089, USA. E-mail: kris658@usc.edu*
[b]*Department of Physics, University of Southern California, Los Angeles, CA 90089, USA*
[c]*Department of Computer Science, University of Southern California, Los Angeles, CA 90089, USA*
[d]*Department of Chemical Engineering and Material Science, University of Southern California, Los Angeles, CA 90089, USA*
[e]*Department of Biological Sciences, University of Southern California, Los Angeles, CA 90089, USA*
[f]*Department of Physics, Kumamoto University, Kumamoto 860-8555, Japan*
†Electronic supplementary information (ESI) available. See DOI: 10.1039/c7nr07890k

mation of chemically-pure dopant-free homojunctions for micro- and nano-patterning of reconfigurable circuits. This is relevant for applications like neuromorphic computing, where the current state-of-the-art relies on thermally-induced structural phase transformation (and associated change in electronic properties) in bulk crystalline and glassy chalcogenides.[25] Electronic excitation is known to induce ultra-rapid bond dissociation and atomic rearrangement in other material systems like graphene,[26] transition metal oxides[27] and polymers[28] and was also shown to introduce large and reversible in-plane atomic displacements in semiconducting monolayers like MoS_2.[29] Recently, Cho *et al.*[30] used laser irradiation to convert $MoTe_2$ monolayers from the H to T′ crystal structure and realized some of these advantages including micron-scale phase patterning and dopant-free homojunction formation. However, this phase transformation was found to be thermally-driven and proceeds primarily by local heating of the $MoTe_2$ sample by the optical pump resulting in the formation of Te vacancies and other point defects. At the same time, several recent experimental pump–probe[29,31] and theoretical[32] studies have been attempted to characterize the ionic potential energy surface and its impact on electron–phonon coupling and resultant atomic dynamics in the excited state.

However, there have been no experimental reports of excitation-driven H → T′ (or T′ → H) phase transformations in this family of materials. Furthermore, the feasibility of using electronic excitation to induce these structural changes has not been investigated theoretically through the quantification of reaction energies and activation barriers. In this work, we use density functional theory calculations to provide a detailed understanding of the mechanism behind lattice distortions resulting from the electronic excitation of a model TMC monolayer of molybdenum telluride ($MoTe_2$). We then investigate the feasibility of using electronic excitation to induce rapid semiconductor-to-metal transitions by quantifying activation barriers for the H → T′ structural phase transformation in $MoTe_2$ monolayers in their ground and excited states. Details about the simulation of ground and excited state crystals are provided in the ESI.† There is significant interest in phase transformations in the $MoTe_2$ material system owing to the relatively small difference between the energies of the H and T′ polytypes, which makes it a suitable candidate material for the investigation of rapid and reversible phase transformations.[4]

H → T′ structural transformation in the ground state

We use climbing image nudged elastic band (CINEB) calculations to quantify the activation barrier for the homogeneous phase transformation between H and T′ crystal structures in the ground state. Atomic structures along the NEB pathway are characterized by three primary displacements.

a. In-plane translation of one plane of Te atoms by ~2 Å along the armchair direction, which transforms the coordination around each central Mo atom from trigonal prismatic to octahedral.

b. Simultaneous in-plane displacement of Mo atoms leading to the formation of Mo–Mo dimer chains as well as twisted/distorted octahedral coordination around Mo atoms.

c. Small out-of-plane displacements of Te atoms lying between dimerizing Mo atoms.

This pathway is informed by the mechanism of the phase transformation observed in experiments on MoS_2 monolayers[22] and is identical to the pathway considered in previous theoretical studies on TMC systems.[33,34]

Time-resolved microscopy of TMC crystals shows that the H–T′ phase transformation in experimental material samples occurs heterogeneously by nucleation and growth from lattice imperfections like vacancies, dislocations, dopants, and 1D defects like edges or boundaries. However, due to the relatively small lateral size of the simulation cells in this study, we restrict our discussion to the case of homogeneous phase transformation between the H and T′ crystal structures, which can be used to qualitatively compare phase transformation kinetics at different levels of excitation.

We calculate an activation barrier, E_a, of 0.77 eV/$MoTe_2$ (Fig. 1), which is comparable to previously reported values of 0.89 eV (ref. 34 and 35) for the $MoTe_2$ monolayer for the same

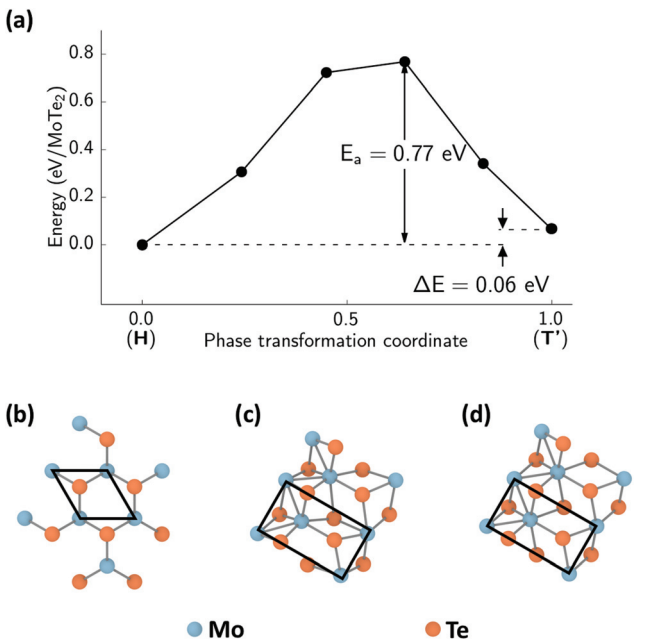

Fig. 1 The energy profile of the $MoTe_2$ monolayer structure (a) along the phase transformation pathway from the H (b) to the T′ (d) phases shows an energy barrier of 0.77 eV at the transition state (c) for the mildly endothermic (ΔE = 0.06 eV/$MoTe_2$) phase transformation process. This barrier, which is much larger than the energy of thermal fluctuations, explains the poor kinetics of the thermally-driven phase transformation. The phase transition coordinate along the NEB pathway is quantified as a normalized mean square displacement of atoms in the NEB image from the ideal $MoTe_2$ H lattice. The unit cells for each crystal structure along the NEB pathway are indicated by black lines in figures (b)–(d).

phase transformation pathway. This kinetic barrier compares favorably to reported barriers in other TMC materials like MoS_2 (1.5 eV–1.88 eV (ref. 16, 36 and 37)). While this difference in kinetic barriers between the material systems can be partially attributed to the greater relative stability of the semiconducting polytype of MoS_2 over its metallic counterpart (by 0.5–0.6 eV/MoS_2 [36,38]), it is notable that a large barrier of 0.77 eV (which is significantly larger than the energy of thermal fluctuations) persists even in $MoTe_2$ where the reaction energy of the H → T′ phase transformation is small (ΔE = 0.06 eV/$MoTe_2$). This relatively large activation energy barrier is indicative of a steep potential energy surface for the atomic motion and large dynamic stability of the H lattice against small atomic displacements. In contrast to previous reports of spatially heterogeneous strain-driven phase transformation,[39] we find that homogeneous tensile or compressive strain only leads to a moderate flattening of the potential energy surface (and a concomitant lowering of vibrational frequencies as shown in Fig. S1†) and the H crystal structure remains dynamically stable under large tensile and compressive strains. This indicates that the barrier for homogeneous phase transformation remains significant even in the strained monolayer.

Electronic structure and dynamical stability upon electronic excitation

Fig. 2a shows the electronic density of states for the ground state $MoTe_2$ monolayer near the valence and conduction band edges (see Fig. S2† for the full density of states), showing a band gap of 1.1 eV, consistent with previous DFT-GGA calculations, and materials databases.[40,41] These bandgap values are also in good agreement with the experimentally measured optical bandgap in $MoTe_2$ monolayers, but this good agreement is likely due to a fortuitous cancellation of errors within the DFT-GGA method.[42] Within the rigid-band ΔSCF formalism of the excited state modeling used in this study, the Fermi level in the $MoTe_2$ monolayer upon vertical electronic excitation can be obtained from the integrated density of states (Fig. 2a, blue) corresponding to the required density of photogenerated charge carriers. Fig. 2b shows contours of the Fermi surface within the first Brillouin zone at two representative excited charge carrier concentrations, n(e–h) = 0.5 × 10^{14} cm^{-2} and n(e–h) = 1.0 × 10^{14} cm^{-2}. The values of n(e–h) explored in this study (of the order of 10^{14} cm^{-2}) are well in line with the experimentally accessible concentration of charge carriers in two-dimensional materials like TMDCs and graphene due to chemicals and photodoping.[14,24] Furthermore, recent pump–probe experiments have demonstrated that similar concentrations of n(e–h) can be sustained in mono- and few-layer TMDCs without causing permanent damage to experimental samples.[43] At low values of n(e–h), corresponding to mild optical excitation, the Fermi surface is localized to pockets at the K-point, consistent with the direct bandgap of the $MoTe_2$ monolayer. At larger values of n(e–h), the Fermi surface also shows features around the Σ-point in the reciprocal space

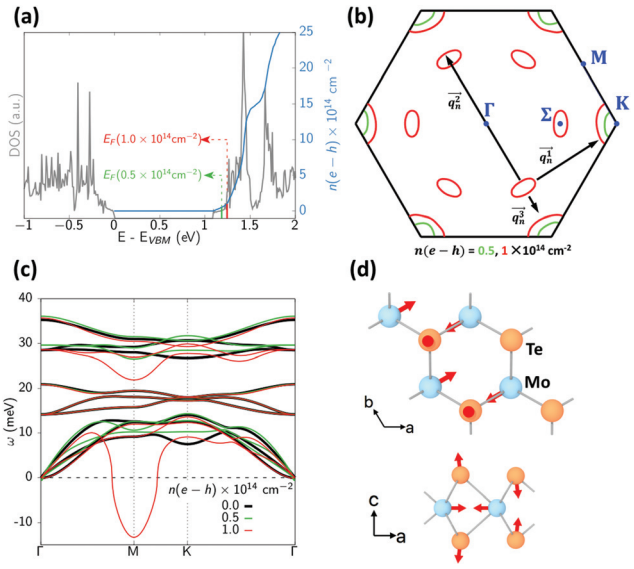

Fig. 2 (a) Density of states for monolayer $MoTe_2$ near the band edge (blue). Integrated density of states (red) is used to calculate the Fermi level for arbitrary values of electronic excitation, n(e–h). (b) Fermi surface for n(e–h) = 0.5 × 10^{14} cm^{-2} to 1 × 10^{14} cm^{-2} plotted within the first Brillouin zone, with high-symmetry points marked in blue. The Fermi surface is localized to the K-point at mild excitation, and exposes Σ-pockets at higher excited charge carrier density. The three nesting vectors, q_1, q_2 and q_3, correspond to reciprocal vectors ΓM, ΓK and ΓΣ, respectively. (c) A plot of the phonon band structure of monolayer $MoTe_2$ at three representative exciton densities (expressed in units of cm^{-2} in the figure) shows that at the critical exciton density of 1 × 10^{14} cm^{-2}, soft vibration modes emerge at the M-point (0.5 0 0) at the boundary of the first Brillouin zone. (d) Eigenvectors of the soft longitudinal acoustic vibration mode at the M point (0.5 0.0 0.0) showing in-plane wrinkling of Mo lattice positions leading to the formation of Mo–Mo dimer chains as well as out-of-plane wrinkling of Te ionic positions.

located between the Γ and K points. These Fermi surface states are connected by nesting vectors $\overrightarrow{q_n^1}$, $\overrightarrow{q_n^2}$ and $\overrightarrow{q_n^3}$, corresponding, respectively, to the coherent scattering of M, K and Σ phonons. This scattering is accompanied by very strong electron–phonon interactions, which can significantly affect the phonon dispersion at these q-points. Similar electron–phonon coupling effects have been observed in other isostructural and isoelectronic crystals like MoS_2 and $MoSe_2$ when the Fermi-level is elevated by electron-doping or electronic excitation.[44]

Fig. 2c shows the phonon dispersion curve of the H $MoTe_2$ crystal at three representative concentrations of excited charge carriers, n(e–h) = 0.0, 0.5, 1.0 × 10^{14} cm^{-2}, corresponding to no, moderate and strong optical excitation. While the ground state $MoTe_2$ H crystal is dynamically stable, consistent with previous studies,[45] we identify a pronounced softening of the longitudinal acoustic vibration mode at the M point (0.5 0 0) at the boundary of the first Brillouin zone at exciton densities equal to and greater than 1.0 × 10^{14} cm^{-2}. This observed softening is qualitatively similar to soft vibration modes observed in electron-doped TMC monolayers.[46] The eigenvector corresponding to this soft mode (Fig. 2c and d) includes periodic inplane displacements of Mo atomic positions with a wave-

length of $\sqrt{3}a$ in the armchair direction, where a is the lattice constant and a corresponding periodic out-of-plane displacement of Te atoms above and below the plane of Mo atoms. These ionic displacements correspond to two of the three primary lattice distortions observed along the NEB pathway from the H to T′ phase. Therefore, this pronounced softening suggests that electronic excitation can reduce the energy of crystal structures along the NEB pathway.

To understand the impact of soft phonon modes on the potential energy surface of $MoTe_2$, we calculate the energy of the excited H crystal as a function of increasing amplitude along the soft-mode eigenvector at different values of the excited charge carrier concentration (Fig. 3). In the absence of significant excitation (*i.e.* n(e–h) = 0–0.5 × 10^{14} cm^{-2}), the potential energy landscape is well described by a single quadratic expression, $E = k{\cdot}x^2$, where x is the magnitude of atomic displacements from the ideal H crystal structure and the effective spring constant, k, is proportional to the calculated phonon frequency at the M-point. Increasing electronic excitation in this regime results in a gradual flattening of the potential energy landscape, which is reflected in a reduction of the spring constant, k, going from $n = 0$ to $n = 0.5 \times 10^{14}$ cm^{-2}. However, higher excitations lead to the destabilization of the H crystal structure leading to a PES which is better described by a quartic equation, $E = k{\cdot}x^2(x^2 - 2x_0{}^2)$, where x_0 is a finite displacement along the soft phonon mode that corresponds to the structure with a minimum energy for the excited crystal.

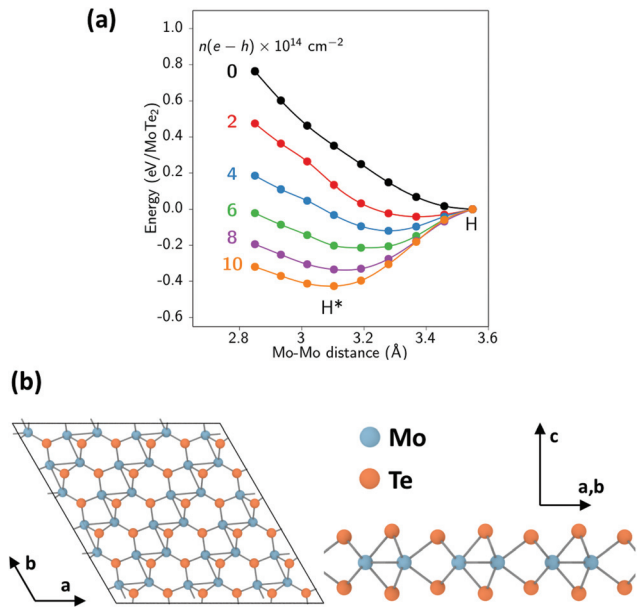

Fig. 3 (a) A plot of energies of the electronically excited crystal as a function of displacement along the soft phonon mode reveals the progressive destabilization of the H crystal structure with increasing density of excited charge carriers and the formation of a metastable ground state (H*) at high exciton densities around 10 × 10^{14} cm^{-2}. (b) The metastable H* crystal structure is characterized by periodic reduction of Mo–Mo bond distances leading to the formation of Mo–Mo dimer chains accompanied by an out-of-plane displacement of Te atoms.

The crystal structure corresponding to x_0 is characterized by shorter Mo–Mo bond distances and the formation of well-defined Mo–Mo dimer chains and the corresponding out-of-plane displacement of Te atoms (Fig. 3b). This crystal structure at the energy minimum is closely related to the H* crystal structure described by Kolobov *et al.*[32] However, as Fig. 3 indicates, H* represents a continuum of crystal structures with differing values of x_0 at different concentrations of excited charge carriers.

H → T′ structural phase transformation in the excited state

In order to identify if the H* crystal structure provides a low-barrier pathway for the H → T′ phase transformation, we quantify the activation barrier between the excited phases of the H and the T′ crystal structures using the CINEB method under the constraint of constant occupancy of excited energy levels.

Fig. 4 compares the calculated activation barriers for the H → T′ structural phase transformation in the ground state to those obtained under intense electronic excitation (n(e–h) = 6–12 × 10^{14} cm^{-2}). The figure shows progressively decreasing barriers for the phase transformation with increasing excited charge carrier concentrations. At n(e–h) = 10 × 10^{14} cm^{-2}, the H* crystal structure is highly destabilized and the calculated activation barrier falls within the energy range of thermal fluctuations, effectively making the phase transformation spontaneous. In addition to changes to the activation barrier, electronic excitation also greatly affects the relative stability of the H and T′ polytypes. While the H is the energetically stable crystal structure in the ground state, the T′ polytype is more stable for n(e–h) values greater than 6 × 10^{14} cm^{-2}. This reversal of stabilities has important implications for the reversibility of the phase transformation. The similarity in the calculated barriers for H → T′ and T′ → H phase transformations in

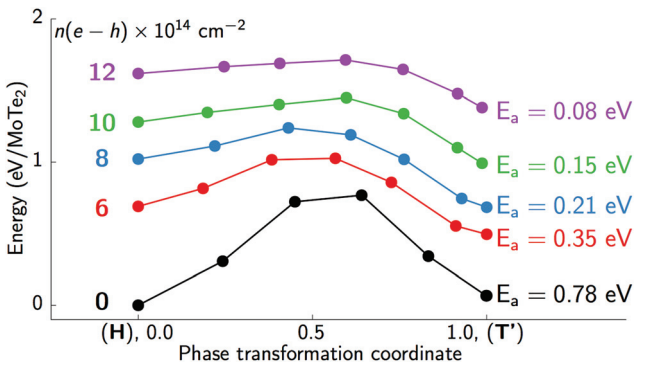

Fig. 4 The plot of DFT energies along the excited-state NEB pathway shows a progressive reduction in the activation barriers for the H → T′ phase transformation with increasing concentration of excited charge carriers. The activation barrier falls within the range of thermal fluctuations for n(e–h) values close to 10 × 10^{14} cm^{-2}. This reduction in barriers is accompanied by destabilization of the H crystal structure relative to the T′ crystal structure.

the ground state (0.77 eV and 0.71 eV, respectively) allows for thermally-excited phase transformation in either direction. However, the strong anisotropy in the barriers in the excited state (0.15 eV and 0.45 eV at n(e–h) = 10×10^{14} cm^{-2}) strongly favors the forward H → T′ phase transformation. This marked difference in the effective barriers for the phase transformation and relative energies of the polytypes in excited and ground state crystals shows that photoexcitation can be an effective method to induce rapid semiconductor-to-metal structural phase transformation in monolayers of TMC materials.

In summary, we have quantified a large activation barrier of 0.77 eV per formula unit for the semiconducting-to-metallic H → T′ structural phase transformation for the model TMC system of $MoTe_2$, which is responsible for the slow kinetics of this transformation in the ground state crystals. We identify Fermi-surface-nesting driven progressive softening of vibration modes at the boundary of the Brillouin zone upon electronic excitation. Lattice distortions corresponding to the eigenvectors of these soft modes lead to the formation of the metastable H* crystal structure as a low-energy intermediate in the conformational space between the H and T′ phases. The activation energy barrier between electronically excited H and T′ crystals decreases monotonically with increasing density of excited charge carriers and reduces to the range of thermal energy fluctuations at charge carrier concentrations beyond 12×10^{14} cm^{-2}. These results suggest that optically induced electronic excitation could be a viable method for rapid, controllable and localized semiconductor-to-metal phase transformation in the TMC monolayer system.

Conflicts of interest

There are no conflicts to declare.

Acknowledgements

This work was supported as part of the Computational Materials Sciences Program funded by the U.S. Department of Energy, Office of Science, Basic Energy Sciences, under Award Number DE-SC00014607. Simulations were performed at the Center for High Performance Computing of the University of Southern California. We would like to thank Dr Uwe Bergmann, Dr Ming-Fu Lin and Dr Clemens Weninger at SLAC National Accelerator Laboratory for helpful discussions about $MoTe_2$ and Prof. Stephan Haas at USC for discussions about excited state calculations.

References

1 S. Manzeli, D. Ovchinnikov, D. Pasquier, O. V. Yazyev and A. Kis, *Nat. Rev. Mater.*, 2017, **2**, 17033.
2 M. Chhowalla, D. Voiry, J. E. Yang, H. S. Shin and K. P. Loh, *MRS Bull.*, 2015, **40**, 585.
3 G. Eda, T. Fujita, H. Yamaguchi, D. Voiry, M. W. Chen and M. Chhowalla, *ACS Nano*, 2012, **6**, 7311.
4 K. A. N. Duerloo, Y. Li and E. J. Reed, *Nat. Commun.*, 2014, **5**, 4214.
5 C. M. Huang, *et al.*, *Nat. Mater.*, 2014, **13**, 1096.
6 S. W. Luo, *et al.*, *Nanotechnology*, 2015, **26**, 105705.
7 A. L. Friedman, F. K. Perkins, A. T. Hanbicki, J. C. Culbertson and P. M. Campbell, *Nanoscale*, 2016, **8**, 11445.
8 R. Kappera, D. Voiry, S. E. Yalcin, B. Branch, G. Gupta, A. D. Mohite and M. Chhowalla, *Nat. Mater.*, 2014, **13**, 1128.
9 D. Voiry, *et al.*, *Nat. Mater.*, 2013, **12**, 850.
10 B. Mortazavi, A. Ostadhossein, T. Rabczuk and A. C. T. van Duin, *Phys. Chem. Chem. Phys.*, 2016, **18**, 23695.
11 X. D. Duan, *et al.*, *Nano Lett.*, 2016, **16**, 264.
12 G. Eda, H. Yamaguchi, D. Voiry, T. Fujita, M. W. Chen and M. Chhowalla, *Nano Lett.*, 2011, **11**, 5111.
13 B. Radisavljevic and A. Kis, *Nat. Mater.*, 2013, **12**, 815.
14 Y. C. Cheng, A. M. Nie, Q. Y. Zhang, L. Y. Gan, R. Shahbazian-Yassar and U. Schwingenschlogl, *ACS Nano*, 2014, **8**, 11447.
15 C. X. Zhang, *et al.*, *ACS Nano*, 2016, **10**, 7370.
16 M. R. Ryzhikov, V. A. Slepkov, S. G. Kozlova, S. P. Gabuda and V. E. Fedorov, *J. Comput. Chem.*, 2015, **36**, 2131.
17 A. N. Enyashin, L. Yadgarov, L. Houben, I. Popov, M. Weidenbach, R. Tenne, M. Bar-Sadan and G. Seifert, *J. Phys. Chem. C*, 2011, **115**, 24586.
18 F. Raffone, C. Ataca, J. C. Grossman and G. Cicero, *J. Phys. Chem. Lett.*, 2016, **7**, 2304.
19 V. Kochat, *et al.*, *Adv. Mater.*, 2017, **29**, 1703754.
20 M. Calandra, *Phys. Rev. B: Condens. Matter Mater. Phys.*, 2013, **88**, 245428.
21 Y. M. Kang, *et al.*, *Adv. Mater.*, 2014, **26**, 6467.
22 Y. C. Lin, D. O. Dumcencon, Y. S. Huang and K. Suenaga, *Nat. Nanotechnol.*, 2014, **9**, 391.
23 Y. Li, K. A. N. Duerloo, K. Wauson and E. J. Reed, *Nat. Commun.*, 2016, **7**, 10671.
24 Y. Wang, *et al.*, *Nature*, 2017, **550**, 487.
25 T. Tuma, A. Pantazi, M. Le Gallo, A. Sebastian and E. Eleftheriou, *Nat. Nanotechnol.*, 2016, **11**, 693.
26 J. Bang, S. Meng, Y. Y. Sun, D. West, Z. G. Wang, F. Gao and S. B. Zhang, *Proc. Natl. Acad. Sci. U. S. A.*, 2013, **110**, 908.
27 G. Kolesov, D. Vinichenko, G. A. Tritsaris, C. M. Friend and E. Kaxiras, *J. Phys. Chem. Lett.*, 2015, **6**, 1624.
28 C. R. Bealing and R. Ramprasad, *J. Chem. Phys.*, 2013, **139**, 174904.
29 E. M. Mannebach, *et al.*, *Nano Lett.*, 2015, **15**, 6889.
30 S. Cho, *et al.*, *Science*, 2015, **349**, 625.
31 L. Waldecker, R. Bertoni, H. Hubener, T. Brumme, T. Vasileiadis, D. Zahn, A. Rubio and R. Ernstorfer, *Phys. Rev. Lett.*, 2017, **119**, 036803.
32 A. V. Kolobov, P. Fons and J. Tominaga, *Phys. Rev. B: Condens. Matter Mater. Phys.*, 2016, **94**, 094114.
33 Y. S. Guo, D. Z. Sun, B. Ouyang, A. Raja, J. Song, T. F. Heinz and L. E. Brus, *Nano Lett.*, 2015, **15**, 5081.

34 C. H. Naylor, *et al.*, *Nano Lett.*, 2016, **16**, 4297.
35 H. H. Huang, X. F. Fan, D. J. Singh, H. Chen, Q. Jiang and W. T. Zheng, *Phys. Chem. Chem. Phys.*, 2016, **18**, 4086.
36 D. N. Esfahani, O. Leenaerts, H. Sahin, B. Partoens and F. M. Peeters, *J. Phys. Chem. C*, 2015, **119**, 10602.
37 M. Pandey, P. Bothra and S. K. Pati, *J. Phys. Chem. C*, 2016, **120**, 3776.
38 X. Y. Guo, G. H. Yang, J. F. Zhang and X. H. Xu, *AIP Adv.*, 2015, **5**, 097174.
39 S. Song, D. H. Keum, S. Cho, D. Perello, Y. Kim and Y. H. Lee, *Nano Lett.*, 2016, **16**, 188.
40 D. M. Guzman and A. Strachan, *J. Appl. Phys.*, 2014, **115**, 243701.
41 A. Jain, *et al.*, *APL Mater.*, 2013, **1**, 011002.
42 C. Ruppert, O. B. Aslan and T. F. Heinz, *Nano Lett.*, 2014, **14**, 6231.
43 M.-F. Lin, *et al.*, *Nat. Commun.*, 2017, **8**, 1745.
44 S. M. Zeng, Y. C. Zhao, G. Li and J. Ni, *Phys. Rev. B: Condens. Matter Mater. Phys.*, 2016, **94**, 024501.
45 Y. U. Li, Y. L. Li, W. W. Sun and R. Ahuja, *Comput. Mater. Sci.*, 2014, **92**, 206.
46 M. Rosner, S. Haas and T. O. Wehling, *Phys. Rev. B: Condens. Matter Mater. Phys.*, 2014, **90**, 245105.